Atmos. Chem. Phys. Discuss., https://doi.org/10.5194/acp-2019-89
Manuscript under review for journal Atmos. Chem. Phys.
Discussion started: 21 March 2019

Secondary organic aerosol formation from photooxidation of furan: effects of NOx and humidity

Xiaotong Jiang[1], Narcisse T. Tsona[1], Long Jia[2], Shijie Liu[1], Hailiang Zhang[2], Yongfu Xu[2], Lin Du[1,*]

[1] Environment Research Institute, Shandong University, Qingdao, 266237, China
[2] State Key Laboratory of Atmospheric Boundary Layer Physics and Atmospheric Chemistry, Institute of Atmospheric Physics, Chinese Academy of Sciences, Beijing, 100029, China

Correspondence to: Lin Du (lindu@sdu.edu.cn)

Abstract. Atmospheric furan is a primary and secondary pollutant in the atmosphere, and its emission contributes to the formation of ultrafine particles and ground-level ozone. We investigate the effects of NOx level and humidity on the formation of secondary organic aerosol (SOA) generated from the photooxidation of furan in the presence of NaCl seed particles. The particle mass concentration and size distribution were determined with a scanning mobility particle sizer (SMPS). SOA mass concentration and yield were determined under different NOx and humidity levels. A significant difference is observed both in the SOA mass concentration and SOA yield variation with the initial experimental conditions. Six organic products were identified in the collected SOA by electrospray ionization exactive orbitrap mass spectrometry (ESI-Exactive-Orbitrap MS). The –COOH, –OH, –C=O and NO_2 functional groups were assigned in the FTIR spectra and used as the indicator for the mechanism inference. In addition, O_3 formation was also observed during the furan-NOx-NaCl photooxidation. Based on the MS analysis, the reaction mechanism was proposed to follow the RO_2+NO pathway. A significant amount of carbonyl-rich products was detected in the SOA products from the photooxidation of furan. The SOA mass concentration and yield increase with increasing humidity, because higher aerosol liquid water content brings more aqueous phase reactions. The present study demonstrates the effect of NOx and humidity on SOA formation during the furan-NOx-NaCl photooxidation. Furthermore, the results illustrate the importance of studying SOA formation over a comprehensive range of environmental conditions. Only such evaluations can induce meaningful SOA mechanisms to be implemented in air quality models.

1 Introduction

Atmospheric particulate matter (PM) does not only have public effects such as human health and life expectancy but also has an adverse influence on visibility and global climate forcing (Hallquist et al., 2009; Pope et al., 2013). PM is primarily composed of organic carbon, black carbon, brown carbon, sulfate, nitrate, and other inorganic components (Donahue et al., 2009; Zhang et al., 2011). Secondary organic aerosols (SOA) constitute a substantial portion of the total ambient aerosol particles, which mainly originate from biomass burning and atmospheric reactions of volatile organic compounds (VOCs) (Kanakidou et al., 2005). Identifying the chemical composition and major precursors of SOA is helpful to better understand their formation mechanism and strategies for the control of PM. Furan is an important five-member heteroatom-containing volatile organic compound present in the atmosphere and it can be produced by wood combustion, oil refining, coal mining and gasification, and pyrolysis of biomass, cellulose, and lignin (Shafizadeh, 1982). As shown in previous studies, furan is one of the most common products of the thermal cracking of biomass (Kahan et al., 2013; Gilman et al., 2015). Both furan and furan-related compounds have been detected in the effluent from initial smouldering of fuels, oats and soft pellets (Olsson, 2006; Perzon, 2010). In addition, furan has been identified as one of the major compounds emitted from the combustion of Ponderosa Pine, which constitute a significant fraction (5-37 % by estimated emission factor) of smoke from combustion (Hatch et al., 2015). Field measurements of hydrocarbon emissions from biomass burning in Brazil have also shown that furans consists of 52% and 72% of the oxygenated hydrocarbons emissions in the cerrado (grasslands) and selva (tropical forest) regions, respectively (Greenberg et al., 1984). Moreover, furan has been proven to be the typical trace gas of roasting/burning activities (Gloess et al., 2014; Coggon et al., 2016; Burling et al., 2010; Gilman et al., 2015; Sarkar et al., 2016; Stockwell et al., 2016; Stockwell et al., 2015; Stockwell et al., 2014), and it is also an important contribution to OH reactivity towards biomass burning emissions (Gilman et al., 2015; Sarkar et al., 2016). Furan is also a secondary pollutant produced in the photooxidation of some conjugate alkenes. Previous product studies of 1,3-butadiene oxidation have shown that furan is one of the dominant product during the OH radical-initiated reactions in the presence of NO (Sprengnether et al., 2002; Tuazon et al., 1999). Furthermore, another source of furan is the cyclization of the unsaturated 1,4-hydroxyaldehydes, which will further go through the dehydration reactions (Baker et al., 2005). There is strong evidence that furan can cause malignant tumor formation in a variety of experimental animals (IARC, 1995). Therefore, a better understanding of the atmospheric transformations of furan will be helpful to improve the air quality models for toxic species.

As an aromatic hydrocarbon, furan is very reactive according to its electrophilic substitution reactions (Villanueva et al., 2007). The measured rate constant of furan with OH radicals, O_3 and NO_3 radicals at room temperature is $(4.01\pm0.30)\times10^{-11}$, $(2.42\pm0.28)\times10^{-18}$ and $(1.4\pm0.2)\times10^{-12}$ cm^3 $molecule^{-1}$ s^{-1}, respectively (Atkinson et al., 1983; Atkinson et al., 1985). If the oxidant concentration of OH and NO_3 are assumed to be 1.6×10^6 and 5×10^8 molecule cm^{-3}, lifetimes of furan for reactions with OH and NO_3 are estimated to be 3 h and 18 min, respectively (Cabanas et al., 2004). In the troposphere, atmospheric furan is expected to be mainly oxidized by OH during daytime and NO_3 at night. Although the determination of kinetics and products of furan oxidation has been performed, SOA formation from furan has not been well characteriszed. It is important to assess the SOA formation potential of furan and its role in SOA production in biomass burning plumes. Although the SOA formation potential of furan has been studied in recent years (Cabanas et al., 2004; Liljegren and Stevens, 2013; Tapia et al., 2011), the influence of several factors including NOx levels and relative humidity (RH) on SOA formation should be further investigated. It is generally accepted that NOx level plays a critical role in SOA formation, by governing the reactions of organo-peroxy radicals (RO_2) (Song et al., 2007; Song et al., 2005). The branching ratio of RO_2 reactions with NOx and the hydroperoxyl radical (HO_2) is determined by the NOx level during experiments (Kroll and Seinfeld, 2008). A previous study showed that the mechanisms of the two reactions differ sharply under different NOx level conditions. RO_2 reacts only with NO under high NOx levels and with HO_2 under low NOx conditions (Ng et al., 2007b). The latter case produces lower volatility products than the former one. The effect of NOx level on SOA formation from aromatic precursors has been investigated previously but the results are inconclusive. A study focusing on the photooxidation of toluene and m-xylene has demonstrated that aerosol yields decrease as NOx level increases (Xu et al., 2015), while another study showed that the SOA yield from photooxidation of isoprene under high-NOx levels is 3 times more important than that measured under low NO_2/NO level (Chan et al., 2010). A different study indicated that under wet conditions, high initial NOx levels contribute effectively to SOA formation (Zhang et al., 2012). This is in agreement with the observation for SOA formation from the irradiation of propylene that showed that the SOA mass yield decreased with increasing propylene/NOx ratio (Ge et al., 2017b).

Besides the mixed effect of NOx level on SOA formation, the RH can significantly alter the sizes of SOA particles, depending on their hygroscopicity (Varutbangkul et al., 2006), their gas-phase reactions involving water (Jonsson et al., 2006), and the aqueous chemistry occurring at their surfaces (Lim et al., 2010; Grgic et al., 2010). The photooxidation experiments of aromatic compounds, such as toluene (Edney et al., 2000; Cao and Jang, 2010; Faust et al., 2017; Hinks et al., 2018), benzene and ethylbenzene (Jia and Xu, 2014), m-xylene (Zhou et al., 2011), and 1,3,5-trimethylbenzene (Cocker et al., 2001) have been carried out previously to study the effect of RH on SOA formation. The results exhibited large discrepancies under different experimental conditions. The yield of SOA generated under low-NOx conditions was found to be small at high RH (Cao and Jang, 2010). A little RH effect was also observed on SOA particle formation and size distributions (Bonn and Moortgat, 2002; Fry et al., 2009). Nevertheless, positive correlations between RH and SOA yield have also been observed in the presence of hygroscopic seed particles (Zhou et al., 2011), and the role of RH in SOA formation also appears to be mixed. Water vapour does not only participate in the VOC photooxidation reactions and affect the gas-phase oxidation mechanisms, but also alters the partitioning of the reaction products between the gas-phase and the particle-phase, hereby influencing the equilibrium partitioning of generated organic aerosols (Spittler et al., 2006). Moreover, the RH is connected with SOA formation due to its strong influence on seed acidity and particle liquid water concentration (Mahowald et al., 2011). A high RH environment contributes to the increase of aerosol liquid water (ALW), which promotes the hydrolysis of organic compounds and leads to other heterogeneous and aqueous phase reactions (Ervens et al., 2011). Previous studies regarding the atmospheric reactions of furan typically focused on the kinetics and mechanism (Gomez Alvarez et al., 2009; Aschmann et al., 2014).

In the present study, we used FTIR, in concert with SMPS to elucidate the roles of NOx level and RH in SOA formation from furan-NOx irradiation. All the experiments were conducted in the presence of NaCl seed particles, which are the second most abundant particles in the atmosphere (Penkett, 1988). NaCl particles acted as the nuclei and took part in secondary reactions. Specifically, we evaluate whether the increased ALW affects the SOA mass concentration and the SOA yield. The chemical composition of furan SOA was investigated by ESI-Exactive-Orbitrap MS, with a focus on the formation of organic nitrates. Strong evidences that both the RH and different NOx levels have a significant effect on SOA formation from furan photooxidation are presented.

2 Experiments

2.1 SOA sample preparation

All experiments were performed in a 1.3 m^3 Teflon FEP film chamber at the Institute of Atmospheric Physics, Chinese Academy of Sciences, Beijing. To maximize and homogenize the interior light intensity, a mirror surface stainless steel was chosen as the interior wall of the enclosure. A total of 42 black-lamps (F40BLB, GE, Fairfield, CT, USA) with emission band centre at 365 nm were equipped in the facilities to simulate the spectrum of the UV band in solar irradiation. The chamber was equipped with multiple sampling ports, which allowed the introduction of clean air, seed aerosols, gas-phase reagents, and for measurements of both gas-phase and particle-phase compositions. The reaction setup used in the present study and the schematic of the smog chamber facility is shown in Fig. S1 (Liu et al., 2017; Jia and Xu, 2014, 2016; Ge et al., 2017a, b).

The zero air (generated from Zero Air Supply, Model 111 and Model 1150, Thermo Scientific) was used as the background gas for the experiments, and three big hydrocarbon traps (BHT-4, Agilent, Santa Clara, CA, USA) coupled with three activated-carbon filters were used to get further purified air. The chamber was cleaned by flowing pure air for at least 4 h prior to each experiment until residual NO, NO_2, O_3 or any other particles could not be detected in the chamber. The prepared gas-phase furan was introduced into the chamber directly by a syringe. A certain amount of NO_2 was injected into the chamber by a gas-tight syringe to achieve the initial NOx level. For the enhancement of the SOA formation, NaCl seed aerosols were injected into the chamber via atomization of NaCl aqueous solution with a constant-rate atomizer (Model 3076, TSI, USA). An aerosol neutralizer (Model 3087, TSI, USA) was used to bring particles to a steady-state charge distribution before they were introduced into the reactor. The initial seed number and mass concentrations were approximately 5×10^4 cm^{-3} and 6 μg m^{-3} on average, respectively. For different RH conditions, the dry zero air was introduced into a bottle of high-purity water to control the humidity of the background air. The humidity in the chamber was detected with a hygrometer (Model 645, Testo AG, Lenzkirch, Germany). Consideration of the rate of furan decay after photooxidation initiation suggests that OH is likely the dominant oxidant for the reaction of introduced furan, and the OH concentration is estimated to be 3. $\times$ 10^7 molecules cm^{-3} in the chamber (Song et al., 2019).The initial experimental conditions considered in this study are summarized in Table 1. Typically, approximate 750 ppb furan was employed. To study the effect of NOx levels on SOA formation, experiments were conducted with initial furan/NOx ratios ranging from 7.8 to 48.1, whereas to develop and test the role of RH, experiments were performed for RH values varying from 5 to 85% and with an initial average furan to NOx ratio of 7.55. The temperature of the chamber was controlled to be 308-310 K during all the experiments.

Particles and gas-phase species may get lost to the chamber walls on short timescales, hereby influencing the gas-phase chemistry and SOA formation. Previous studies determined wall loss rate constants of 4.1×10^{-7}, 3.3×10^{-7} and 3.6×10^{-5} s^{-1} for gaseous NO_2, O_3 and aerosol particles, respectively for the set-up used here (Ge et al., 2016, 2017a). These values are applied in the present study. However, no wall loss of furan was observed within the uncertainty of the detection of the instrument. Furthermore, the light intensity in the reactor was determined to be 0.34 min^{-1} by using the NO_2 photolysis rate constant as the indirect representation. Before the start of each experiment, the static electricity of the Teflon chamber was removed. After all the reactants flowed into the chamber, the reactor was maintained in the dark for at least 40 min without any activities to reach homogeneous mixing.

2.2 Gas and particle monitoring

The concentrations of O_3 and NOx were measured continuously by UV photometric O_3 analyser (Model 49C, Thermo Environmental Instruments Inc.) and a chemiluminescence analyzer (Model 42C, Thermo Electron Corporation, USA), respectively. The sampling flow rate was 1 L min^{-1} for both O_3 and NOx analysers. The uncertainty in the gas-phase measurements was below ± 1 %. The experiment samples were collected by Tenax absorption tubes (150 mm length × 6 mm O.D., 0.2 g sorbent). Furan concentrations and product samples were detected by thermal desorption-gas chromatography-mass spectrometry (TD-GC-MS): the thermal desorber (Master TD, Dani, Italy) was combined with gas chromatography (Model 7890A, Agilent Tech., USA) interfaced to a mass selective detector (5975C, Agilent Tech., USA). The initial reactants concentrations are given in Table 1. The chromatographic analytical method used for the analysis was as follows: the chromatographic column was kept at 338 K for 4 min, then heated to 598 K at a heating rate of 20 K min^{-1} and held for 5 min. The particle size distribution and mass concentration were measured with a scanning mobility particle sizer (SMPS, Model 3936, TSI, USA) composed of a TSI 3081 differential mobility analyser (DMA) and a TSI 3776 condensation particle counter (CPC). The sampling and sheath flow rates of the SMPS were 0.3 L min^{-1} and 3 L min^{-1}, respectively. Given this flow conditions of the SMPS, particle sizes (in counts cm^{-3}) were recorded in 64 size bins for particles in the 13.6 to 710.5 nm size range. The accuracy of the particle number concentration is ±10 % at $<3\times10^5$ cm^{-3}. The method of the reduced Dry-Ambient Size spectrometer (DASS) was used to detect the ALW (Engelhart et al., 2011). To get dry particle mass concentrations, a large diameter Nafion dryer (Permapure MD-700-48F-3) and a multi-tube Nafion dryer (Permapure PD-200T-24E-M) were added to the sampling inlet and sheath flow, respectively. This DASS method is generally accepted and widely used in the detection of ALW content, and can remove up to 90% of the water vapour without losing the organic-bound water. The results were compared with the mass concentrations detected in humid mode, in which the humid air in the chamber was introduced into the SMPS with the sheath air set at 10 L min^{-1}. The ALW was calculated as the difference between the particle mass concentrations determined at dry and humid modes (Jia and Xu, 2018). On the basis of the recorded particle volume concentration and assumed particle density, a total suspended particulate (TSP in µg m^{-3}) could be translated. As shown in Eq. (1), TSP is the sum of seed aerosol (NaCl in this work), $NaNO_3$, particle ALW, and SOA. By dissolving the SOA collected on ZnSe disks into high purity water, an ion chromatograph (IC, Dionex ICS-900, Thermo Fisher, USA) was then used to analyse the inorganic content (Cl^- and NO_3^-) in SOA. With known initial NaCl seed aerosols and their decay rates, the particle mass concentration of NaCl can be calculated, and based on the detected ALW during experiments, the SOA produced in the photooxidation of furan can be estimated from Eq. (1).

$$\mathrm{TSP} = \mathrm{NaCl} + \mathrm{NaNO_3} + \mathrm{ALW} + \mathrm{SOA} \tag{1}$$

2.3 Chemical characterization of products

The SOA particles were sampled on ungreased ZnSe disk (25 mm in diameter) using a Dekati low-pressure impactor (DLPI, Dekati Ltd., Kangasala, Finland) after the appearance of the O_3 maximum concentration. The sampling flow rate of DLPI was 10 L min^{-1} with the particles sizes from 30 nm to 10 μm, classified into 13 stages. According to the particle distribution explored from the SMPS, the SOA particles size was mainly around 150 nm after 3 h of irradiation. The ZnSe disk was placed on stage 3 to reach the maximum collection of the particles. Afterward, the ZnSe disk was put in the FTIR (Nicolet iS10, Thermos Fisher, USA) sample holder, which had been flushed with N_2 to eliminate the impact of ambient H_2O and CO_2 on the determination of the chemical composition of formed SOA particles. The spectra were recorded at 4 cm^{-1} resolution with 128 scans. The samples collected on the ZnSe disk were then dissolved with high purity water for analysing inorganic species.

To obtain chemical characterization information, the electrospray ionization exactive orbitrap mass spectrometry (ESI-Exactive-Orbitrap MS, Thermo Fisher, USA) was also used for the analysis of water-soluble organic aerosol (OA) produced from the photooxidation of furan. As a “soft ionization”, ESI can provide molecular formulae for thousands of OA substances when coupled with a high-resolution mass analyser. The mass resolution is 10^5. The collected SOA samples were eluted with 1 mL of acetonitrile. A total volume of 300 L was sampled at a flow rate of 10 L min^{-1} and a volume of 5 μL of the extraction was used, through a direct injection, for the measurement. The addition of acetonitrile allows a lower surface tension of the solution and provides a stable electrospray ionization process (Koch et al., 2005). Both positive (+) and negative (-) ion modes were chosen to operate. N_2 was used as the sheath and auxiliary gas. The desolvation gas temperature was 320 ℃, and the gas flow was 200 μL min^{-1}. The capture voltage was set to 3 kV.

3 Results and discussion

3.1 Gas phase and SMPS results

Experiments were divided into three groups, which were set to study the role of (i) NOx and (ii) RH on SOA formation, and (iii) to analyze the SOA composition. To keep the variables of each set of conditions consistent, almost identical initial gas phase conditions were required. The addition of furan and seed aerosol in all the experiments was nearly equal. The first set of experiments (Exp.1-6, Table 1), designed to investigate the effect of NOx level on SOA formation, used similar RH conditions with different NOx concentrations. For Exp.6-12, different RH levels coupled with similar furan/NOx ratios were monitored to assess the RH impact on SOA formation. Three experimental conditions were considered to analyse the ESI-Exactive-Orbitrap MS, which intended to compare the role of NOx and RH on the SOA formation. The major gas-phase inorganic chemical reactions occurred during the experiments are presented in Fig. 1. After turning on the light, the photolysis of NO_2 produced NO and O, which further reacted with O_2 to form O_3 in the chamber. As a result, a slight increase in the beginning, followed by the decrease of NO concentrations are observed (Fig. S2). On one hand, the decrease of NO is caused by the reaction between NO and alkyl RO_2, which are formed from the OH-initiated oxidation of furan during the experiment. On the other hand, the oxidation of NO by O_3 also contributes to the NO decreasing trend.

The photochemical oxidation of VOCs in the presence of NOx and OH radical is an important source of tropospheric O_3 (Labouze et al., 2004). Although the atmospheric degradation mechanisms of furan is complex, the fundamental features of troposphere O_3 formation is relatively simple. The main formation pathway of O_3 in the atmosphere is the photolysis of NO_2 as presented in Fig. 1 (R1 and R2). The RO_2 and HO_2 radicals generated from the photooxidation of furan can further react with NO to form NO_2 (R5 and R6), whose photolysis will produce the ground-state oxygen atom (R1) and thus contribute to the net O_3 formation through the reaction of O_2 with O (R2). The very similar VOCs level may result in a high O_3 production with higher NOx concentrations conditions (Bowman and Seinfeld, 1994). As presented in a previous work of the ethylene-NOx-NaCl irradiations, both experimental results and model simulations showed an abundant O_3 production (approximately 500 ppb) with an initial NOx level of 142 ppb (Jia and Xu, 2016). Therefore, it is important to evaluate the O_3 production potential of VOCs in the atmosphere. As shown in Fig. S2, it shows a consistent increasing trend between O_3 concentration and SOA mass concentration, indicating that O_3 was generated during the furan photooxidation reactions with the formation of SOA.

The O_3 maximum concentration, SOA mass concentration and SOA yield dependences on the C_4H_4O/NOx ratio are presented in Fig. 2. The results show that the O_3 maximum concentration produced during the experiments decreases with increasing C_4H_4O/NOx ratio. When the C_4H_4O/NOx ratio decreases from 16.9 to 7.8, there is a sharp increase in O_3 concentration from 197 to 382 ppb. Interestingly, experiments for which the C_4H_4O/NOx ratio changed from 48.1 to 36.60 exhibit a change of 24 ppb in O_3 maximum concentration. This result indicates that under different C_4H_4O/NOx ratio regimes, the concentration of O_3 produced varies much. There is a great change in O_3 accumulation when the C_4H_4O/NOx ratios are relatively low (<16.9), which is consistent with a previous observation from C_3H_6-NOx-NaCl irradiation experiments by Ge et al. (Ge et al., 2017b) who found that when the C_3H_6/NOx ratio was less than 11, the O_3 concentration decreased considerably with increasing ratio, whereas when the ratio was larger than 11, the O_3 concentration slightly decreased with increasing ratio. Fig. S3 shows the comparisons of the observed concentrations of O_3 and NOx from furan irradiations at different experimental conditions. With similar NOx level, the amount of O_3 formed at 5% RH was larger than that at 42% RH. The O_3 maximum concentration was reduced by almost 60% as the C_4H_4O/NOx ratio increased from 7.8 to 36.6. However, the effect of RH on O_3 formation is not so obvious compared to the difference in initial C_4H_4O/NOx ratio. The influence of NOx level on O_3 is likely related to its formation mechanism. The formation of O_3 is directly connected with the NOx in two ways: the photolysis of NO_2, producing the O atom that reacts with O_2, and the NOx reacting directly with RO. However, the RH has little to no effect on O_3 formation. This formation is slightly favoured at low RH whereas, at high RH, the NO_2- and ONO_2- are easily transferred into the aerosol phase, thereby suppressing the O_3 formation (Jia and Xu, 2014). The appearance time of O_3 maximum concentration at high C_4H_4O/NOx ratio is almost half an hour earlier than that at low initial C_4H_4O/NOx ratio. On the contrary, there is no significant difference in the balance time of NOx concentration under different experimental conditions. Similar initial C_4H_4O/NOx ratios result in a similar profile of NOx concentration during the experiment, although the final

NOx concentration shows a slight difference. The dependences of O_3 maximum concentration on RH are presented in Fig. 3. The O_3 maximum concentration was detected in each experiment. The O_3 maximum concentration decreased with increasing RH, whereas the SOA mass concentration and yield increased. This decrease in O_3 maximum concentration is likely due to the fact that high RH conditions favour the transformation of polar nitro (RNO_2) and nitrate ($RONO_2$) into the aerosol phase (reaction (R10)), which suppressed the reaction of RO and NO_2, thus decreased the O_3 formation through the pathways of reactions (R1) and (R2) (Jia and Xu, 2016). Another possible explanation for this decrease might be the heterogeneous reaction of N_2O_5 with aerosol liquid water and NaCl particles as demonstrated by a previous work (Jia and Xu, 2014).

The calculated SOA yield is defined as the ratio of the mass concentrations of the maximum SOA formed (M_{SOA} in µg m^{-3}, corrected by wall loss) and the reacted furan (ΔC_4H_4O in µg m^{-3}):

$$Y_{SOA} = (M_{SOA}/\Delta C_4H_4O) \times 100\ \% \tag{2}$$

where M_{SOA} is obtained by subtracting the amount of NaCl and $NaNO_3$ from the total particle mass concentration measured by the SMPS, and ΔC_4H_4O is the consumption of furan during the experiments. Experiments were started with an average of 6 µg m^{-3} of NaCl seed aerosol and were conducted under different initial C_4H_4O/NOx ratios. After the photooxidation reactions, the SOA mass concentrations reached maxima between 1.0 and 23.5 µg m^{-3}, with SOA yield ranging from 0.04% to 1.01%. In other experiments carried out under varying RH conditions, SOA maxima were in the range of 23.5-119.2 µg m^{-3}, with SOA yield ranging from 1.01% to 5.03%.

3.2 SOA chemical composition

To get detailed information on the functional groups in SOA formed during the photooxidation of furan, the collected particles were measured by FTIR, which has been proven to be an ideal technique for the detection of functional groups and bond information in aerosol samples. The FTIR spectra of particles collected from furan-NOx-NaCl with different values of C_4H_4O/NOx ratio are shown in Fig. 4. The absorptions of organic functional groups were detected, which further confirmed the SOA formation from the photooxidation of furan. The assignment of the FTIR absorption frequencies is summarized in Table 2. The organic nitrate exhibits typical NO symmetric stretching at 868 cm^{-1}, NO_2 symmetric stretching at around 1341 cm^{-1}, and NO_2 asymmetric stretching at 1614 cm^{-1} (Jia and Xu, 2016). The absorption at 1067 cm^{-1} matches the C-O stretching vibration in C-O-C, while the sharp absorption at 1724 cm^{-1} is the C=O stretching vibration in carboxylic acid and ketones (Sakamoto et al., 2013). The carbon skeleton corresponds to the vibrations between 2850 cm^{-1} and 3100 cm^{-1}, where the ν(C-H) stretching vibration can be found. Absorptions in the ranges 2850-3000 cm^{-1} and 3000-3100 cm^{-1} represent the C-H stretching vibration in saturated carbon ring and unsaturated alkenes, respectively. Correspondingly, the C-H bending vibrations are represented by the absorption between 1350 and 1515 cm^{-1}. The strong broad vibrations at 2400-3500 cm^{-1} are interpreted as the O-H stretching vibration in carboxyl groups and hydroxyl groups (Ge et al., 2017b).

Fig. 4 illustrates the influence of NOx level on the SOA components during the photooxidation of furan. For each of the functional groups, experiments with the most pronounced SOA formation are those with the lowest initial C_4H_4O/NOx ratio. This is further confirmed by comparing the SOA yield for different NOx level conditions under approximately similar gas-phase and initial seed conditions. The calculated variations of the relative abundance of FTIR functional groups at different NOx levels are presented in Fig. S5, in which the absolute abundances are normalized with respect to the corresponding functional abundance detected at C_4H_4O/NOx=7.8. The carbonyl compound formed with 7.8 initial C_4H_4O/NOx ratio is approximately thrice more abundant than that formed with 48.1 initial C_4H_4O/NOx ratio. The absorbance of NO_2 functional groups exhibits a much stronger enhancement under initial C_4H_4O/NOx ratio of 7.8 compared to 48.1. Although at different C_4H_4O/NOx ratio conditions the intensities of C-O-C and O-H functional groups show similar trends, their variations are substantially different from the variations of other functional groups. In sum, the increased absorbance of functional groups with decreasing initial C_4H_4O/NOx ratios demonstrates that relatively high NOx level contributes to the formation of SOA.

The FTIR results in the investigation of furan photooxidation under different RH conditions are shown in Fig. 5. The absorbance of FTIR characteristic peak increases with the RH raising from 5% to 85%. Note that obvious intensities of the functional groups were observed when the RH exceeded the efflorescence RH of NaCl. In contrast, the absorptions of corresponding functional groups enhance gently when the RH is lower than 42%. This phenomenon is consistent with the results of the SOA yield discussed above and, can also be interpreted as the increasing ALW components contributing to SOA formation. The ratio of the absorbance intensities detected at low RH to that at 85% RH is used as the relative abundance to show more intuitive FTIR results. As shown in Fig. S6, for RH between 5% and 37%, the intensities of all functional groups vary weakly and are approximately one-third of the intensity at 85% RH. However, when the RH rises from 42% to 85%, the absorption intensities of O-H and NO_2 functional groups increase by factors of 2.0 and 1.9, respectively. In this RH range, the variations of relative intensities are even stronger for C=O, C-H and C-O-C, being increased by factors of 2.3, 2.3 and 2.5, respectively. A previous study has observed that in an urban environment containing aromatic hydrocarbons and NOx, the SOA yield increased by a factor of 2 to 3 under high RH compared to lower RH (Zhou et al., 2011). This trend is similar to that found in experiments with toluene in an urban aromatic hydrocarbon-NOx mixture system (Kamens et al., 2011). It should be pointed out that observed FTIR results show a high degree of consistency with the SOA mass concentration and SOA yield.

To further identify and confirm the structure of generated SOA components, more techniques, such as GC/MS and ESI-Exactive-Orbitrap MS were used to analyse the chemical composition. The chromatography before ESI-MS analyses is helpful to remove the disturbances of the inorganic salts and determine the appropriate molecular compound (Surratt et al., 2007; Gao et al., 2006). However, the collected PM products were not sufficient for the chromatography owing to the limitation of the chamber volume. Furthermore, the low SOA yield of the furan photooxidation make it harder to remain enough SOA components for the better response of ESI-MS signal. Consequently, direct infusion analyses were carried out for ESI-Exactive-Orbitrap MS in the present study. The first-generation products produced by the photooxidation of furan are not expected to partition directly into the particle phase according to their volatilities. Three experiments of furan-NOx-NaCl photooxidation that were conducted under different initial C_4H_4O/NOx ratios and RH conditions were analysed by ESI-

Exactive-Orbitrap MS, and the MS spectra of generated species are shown in Fig. 6. The mass spectra recorded in different ion modes represent the detected compounds ionisable in either positive or negative modes (Walser et al., 2008). Although not reported here, we found that experiments performed at a relatively high initial C_4H_4O/NOx ratio (16.2) and high RH (79%) conditions exhibit similar SOA components to those detected in the experiments performed under 7.3 initial C_4H_4O/NOx ratio and 5% RH conditions. At 5% RH, the chromatographic peaks obtained at C_4H_4O/NOx ratio of 7.3 were found to be more intense than those obtained at 16.2. This is an indication that a relatively high NOx level contributes more to the SOA mass, however, without changing the composition of the SOA components. The peak intensities changes of SOA products detected in the positive mode were not obvious. However, increasing the RH resulted in an overall addition of peak intensities in the negative ion mode, due to the fact that the sample obtained at high RH during the SOA generation had a larger particle mass. For example, a relatively stronger intense band of $C_4H_4O_4Cl_2$ component (m/z=187) was found under a high RH. It is possible that the aqueous surface of seed particles provides a new substrate for the photooxidation of furan. Previously, N_2O_5 and HNO_3 have been proven to be the key products in the VOC-NOx irradiation experiments (Wang et al., 2016). Furthermore, with the formation of acid components as shown in the FTIR results, acid-catalysed reactions may occur during the experiment, which will promote the uptake of the semi-volatile products generated from the photooxidation of furan. Previous studies found that the uptake by acid-catalysed reactions contributed to the formation of SOA (Riva et al., 2016; Lin et al., 2012). Fig. 7 shows the sum of the ion mass peaks with *m/z* ranges in <200, 200-299, 300-399 and 400-499. The signals with *m/z* = 200-299 were more intense than the signals in other *m/z* ranges, for both positive and negative ion modes. Despite the changing of peak abundance, the major observed mass spectra peaks remained the same. Table S1 lists the identified compounds in each ion mode under different experimental conditions.

3.3 Effects of NOx on SOA formation

To study the NOx level effect on SOA formation from the photooxidation of furan, the experiments were conducted with varying initial C_4H_4O/NOx ratios ranging from 7.8 to 48.1. The SOA formation is found to have much lower yield under a high C_4H_4O/NOx ratio. The SOA mass concentration and SOA yield increased from 1.0 to 23.5 $\mu g\ m^{-3}$ and 0.04% to 1.01%, respectively, as the initial concentration ratio of C_4H_4O/NOx decreased from 48.1 to 7.8 (ppbC/ppb). This trend is consistent with previous studies on propylene photooxidation, which found that the SOA yield was enhanced under a low VOC/NOx ratio (Ge et al., 2017b). Another laboratory study of aerosol assessment from isoprene photooxidation concluded that under low NOx level (< 129 ppb), the SOA mass increased with increasing initial NOx level (Kroll et al., 2006). By comparing the studies of Ge et al. and Kroll et al., there is a positive correlation between NOx effect and SOA formation when the initial NOx level is relatively low (nearly below 100 ppb). These results further support our findings in the experiments of furan photooxidation. As shown in Fig. S4, SOA formed under a low C_4H_4O/NOx ratio also have a faster increase than those under large C_4H_4O/NOx ratio conditions. However, the particle number distribution under C_4H_4O/NOx=7.8 and C_4H_4O/NOx=36.6 conditions shows similar profiles.

According to the identified products in this work and based on previous kinetic (Atkinson et al., 1983; Lee and Tang, 1982) and products (Villanueva et al., 2009; Aschmann et al., 2014; Tapia et al., 2011; Villanueva et al., 2007; Strollo and Ziemann, 2013) studies, a proposed chemical mechanism for SOA formation from furan in the presence of NOx is shown in Scheme 1. Additionally, on the basis of well-established mechanisms for atmospheric volatile organic compounds (Atkinson and Arey, 2003), it can be concluded that the reaction is initiated by OH addition to a C=C bond at C2 or C3 positions. Addition at the C2 position forms two cyclic alkyl radicals (a, c), one of which (a) can isomerize to form a ring-opened alkyl radical (d), whereas addition at the C3 position forms a single alkyl radical (b). The OH radical addition leading to an hydrogen abstraction generates the alkyl radicals (R·) followed by reaction with O_2 to form alkylperoxy radicals ($RO_2\cdot$) (Pan and Wang, 2014). The ring-opened alkylperoxy radical generated from (d) can decompose to generate an unsaturated 1,4-dialdehyde (A). Moreover, the formed alkylperoxy radicals ($RO_2\cdot$) can either react with RO_2/HO_2 or NO to yield the corresponding alkoxy radical (RO·), which can (i) react with NO/O_2 to form a first-generation peroxydinitrate compound (m/z = 157) (Atkinson, 2000), (ii) react with O_2 to form a first-generation unsaturated products 1,4-aldoacid (B) and hydroxyfuranone (C), or (iii) decompose and then react with O_2 to yield a 1,4-aldoester (D). It is worth mentioning that the hydroxyfuranone (C) can go through a ring-opening reaction via acid-catalyzed heterogeneous/multiphase reactions to form the unsaturated 1,4-aldoacid (B). Scheme 1 also shows the formation of second-generation products (E) and (F) via reactions of the hydroxyfuranone (C) with 1,4-dialdehyde (A) and 1,4-aldoester (D), respectively. As detected by the ESI-Exactive-Orbitrap MS, the hydroxynitrates (m/z = 194, 281) were generated by the reactions of first products with OH radicals and $O_2/NO/NO_2$ (Carlton et al., 2009; Ervens et al., 2011). There are two pathways for hydroxynitrates formation from RO_2 radicals in the presence of NOx according to which RO_2 radicals may react with NO and NO_2 to form $RONO_2$ and $ROONO_2$, respectively (Kroll and Seinfeld, 2008). However, the formed peroxynitrates could easily thermally dissociate and convert to $RONO_2$. There is a possibility that the SOA products will combine the NaCl seed by ion-clustering interactions. This speculation was further confirmed by the analysis of FTIR results. The absorption of C-Cl functional group can not be assigned in FTIR spectra, which demonstrates that there was no chlorinated organic compounds formed during furan photooxidation. Therefore, the identified chlorine containing organic compounds (m/z=187.04, 255.23, 281.24) in negative ion mode were probably generated from the Cl adduction of SOA product.

As discussed above, the SOA yields increased with the increase of the NOx concentration in the present study. Generally, the NOx level has two different effects in the reaction process. Firstly, increasing NOx concentration will promote the O_3 and HONO formation, leading to more OH radical formed, which in turns is favorable to SOA formation (Sarrafzadeh et al., 2016). In addition, sufficient NOx can facilitate the competition between NO and HO_2 to react with RO_2. Products with high volatility will be generated more by the $NO+RO_2$ reaction than by HO_2+RO_2 reaction (Kroll and Seinfeld, 2008). However, the formation of lower volatility products favors the increase of SOA yields (Chen et al., 2018). In this regard, the increasing NOx level is not conducive to SOA formation. It was shown that the yields of SOA generated from the photooxidation of *m*-xylene increased firstly and then decreased with the increase of the NOx level (Chen et al., 2018). As a result, the effect of NOx level on SOA formation could be different under different conditions: if the NOx level do not reach the critical values of $NO+RO_2$ dominant reactions, the increasing NOx level is likely to promote the SOA formation, otherwise, the $NO+RO_2$ reaction path will restrain the SOA formation. However, in the present study, an increasing trend of SOA formation was observed with the increase of NO concentration. As shown in the ESI-Exactive-Orbitrap MS results, all the detected primary products are carbonyl-rich, and even the organonitrates have at least two carbonyl functional groups. These carbonyl-containing products have lower volatility and contribute to the SOA formation. The peak intensity in the MS of the product (m/z=194) generated by HO_2 pathway (as indicated by the scheme 1) decreased with the increase of NO concentration. However, other products with highly oxygenated molecules exhibit positive correlations between NO concentration and MS peak intensity. This result supports the possibility that the main fate of RO_2 is mainly through reaction with NO. Consequently, we did not observe a decreasing trend of SOA yield as the NOx level increases, which is different from the photooxidation of other aromatic compounds where increasing NOx concentration suppresses the SOA formation (Deng et al., 2017; Ng et al., 2007a).

3.4 Effect of RH on SOA formation

Experiments 6-12 were conducted under seven different RH conditions. Under different RH conditions ranging from 5% to 85%, the SOA yield increases from 1.01% to 5.03%. With almost identical initial conditions except for RH, furan-derived SOA formed at high RH can be a factor of two higher than that formed at low RH. A similar trend was also observed by Yu et al., who found that the SOA mass concentrations increased by a factor of six when RH increased from 18% to 82% (Yu et al., 2011). This phenomenon might result from the SOA formation through heterogeneous reactions and aqueous chemistry in wet aerosols (Grgic et al., 2010; Lim et al., 2010). In these atmospheric processes, alcohols, aldehydes, and ketones formed from the photooxidation of furan in the gas phase can be absorbed into the humid surface of the hygroscopic SOA at high RH. This further contributes to the formation of low-volatility products on the SOA surface. An obvious increase of SOA yield was observed when the RH increased from 37% to 42%. This phenomenon was mainly caused by the efflorescence transition when the seed particles were coated with SOA. It has been previously shown that SOA formation decreases both the efflorescence RH and deliquescence RH of the seed particles and results in the uptake of water by the particles (Liu et al., 2018; Takahama et al., 2007; Smith et al., 2012). There is a high possibility that the NaCl seeds effloresce early after being coated by the new formed SOA. The effect of efflorescence contributes to the water uptake by the particles, leading to the obvious trend-changing of SOA yield. It is noted that with the NaCl seed aerosols serving as nuclei, the ALW was more generated at higher RH. Products with water solubility produced from the photooxidation of furan can dissolve into the ALW on the surface of particle aerosols. As a result, ALW in the formed aerosols plays an important role in gas/particle partitioning. As shown in Fig. 3, the ALW was detected when the RH was higher than 54%, which was based on the deliquescence of NaCl under high RH conditions. The increase of ALW could partially explain the increase of SOA mass concentration and SOA yield. It is highly probable that the particle surface area increases with the amount of ALW increasing, which likely promotes the dissolution of semi-volatile matters produced during the experiments. In addition, the aqueous photochemistry of highly soluble small compounds that portioned in ALW could produce additional organic compounds and result in larger SOA yield under high RH conditions (Faust et al., 2017; Jia and Xu, 2014). Therefore, it is possible that at high RH the produced SOA could partition into wet particle seeds and further contribute to air pollution. Contour plots of SOA bursts in Fig. S4 show that SOA is very quickly generated under high RH conditions with a wide particle diameter distribution.

The effect of RH on SOA formation in furan photooxidation is dominantly determined by the aqueous photochemistry under high RH conditions as discussed above. The heterogeneous reactions including acid catalyzed reactions at the surface of particles promote the formation of first-generation gloxal-like products, which likely play an important role in the process of SOA formation. Moreover, the moist surface under high RH conditions is more favorable for the condensation of the products with low vapor pressure, leading to the increasing production of SOA formation. The proposed gloxal-like compound (D) plays a substantial role in the obvious increasing of m/z=187 product formation under high RH conditions. A decreasing intensity of m/z=255 product was also observed with more m/z=187 product formation. As shown in Scheme 1, there is a competition between these two products from the gloxal-like compound (D). The high RH environment favors the formation of m/z=187 product, leading to the opposite trend of MS peak intensity of these two products. Previously, unsaturated first-generation reaction products of 3-methyl furan have also been suggested to undergo acid-catalyzed condensed-phase reactions, with SOA yields up to 15% (Strollo and Ziemann, 2013). In addition, the reinforced effect of RH on SOA yield was also ascribed from the photooxidations of other aromatic compounds, such as, benzene (Ng et al., 2007c), toluene (Hildebrandt et al., 2009; Kamens et al., 2011), and xylene (Zhou et al., 2011).

4 Conclusions

The effects of NOx and RH on SOA formation from the photooxidation of furan in the presence of NaCl seed particles have been investigated in this study. The results demonstrated that the formation of SOA were promoted when the initial VOC/NOx ratio decreases. The reason for the promotion of SOA mass at a low furan/NOx ratio is that more carbonyl-rich products were generated from the furan photooxidation, which contributes to the formation of SOA. Additionally, the increase of RH results in the increase in the mass concentration of the produced SOA. The mechanisms controlling SOA formation may include the gas-phase photooxidation of furan, physical water uptake as RH increases, and the gas-phase reaction of water with the first-generation products and the aqueous chemistry of low-volatility products reacting at the wet surface of NaCl seed particles. Seed aerosols are important for the growth of atmospheric particles and, therefore, affect aerosol-cloud-climate interactions. Organic nitrates, detected with FTIR and ESI-Exactive-Orbitrap MS, were found as significant composition of newly formed particles. The O_3 formation accompanying with the SOA formation were also observed during the furan-NOx-NaCl photooxidation, which suggests a significant O_3 formation potential of atmospheric furan. A recent study showed that the reactive nitrogen chemistry in aerosol water can be a source of atmospheric sulfate during haze events (Cheng et al., 2016). In addition, the ALW is deeply linked with air quality (Malm et al., 1994) and aqueous SOA formation (Sareen et al., 2017). The influence of the ALW component on SOA yield was examined and it was found that increased ALW amounts lead to higher SOA mass concentration and yield, therefore highlighting the importance of the ALW in photooxidation reactions. ALW plays a crucial role in atmospheric physicochemical processes. The current results could also be used to interpret ambient gas-phase measurements and reaction mechanisms inference.

The Supplement related to this article is available online.

Author contributions

LD and XJ conceived and led the studies. XJ, NT, LJ, SL and HZ carried out the experiments and analysed the data. XJ, LD and SL interpreted the results. NT, LJ and YX discussed the results and commented on the manuscript. XJ prepared the manuscript with contributions from all co-authors.

Competing interests

The authors declare that they have no conflict of interest.

Acknowledgments

This work was supported by National Natural Science Foundation of China (91644214, 41375129), Shandong Natural Science Foundation for Distinguished Young Scholars (JQ201705), Shandong Key R&D Program (2018GSF117040), and Fundamental Research Funds of Shandong University (2017JQ01).

References

Aschmann, S. M., Nishino, N., Arey, J., and Atkinson, R.: Products of the OH radical initiated reactions of furan, 2-and 3-methylfuran, and 2,3-and 2,5-dimethylfuran in the presence of NO, J. Phys. Chem. A, 118, 457-466, 10.1021/jp410345k, 2014.
Atkinson, R., Aschmann, S. M., and Carter, W. P.: Kinetics of the reactions of O_3 and OH radicals with furan and thiophene at 298±2 K, Int. J. Chem. Kinet., 15, 51-61, 0.1002/kin.550150106, 1983.
Atkinson, R., Aschmann, S. M., Winer, A. M., and Carter, W. P.: Rate constants for the gas-phase reactions of nitrate radicals with furan, thiophene, and pyrrole at 295±1 K and atmospheric pressure, Environ. Sci. Technol., 19, 87-90, 0013-936X/85/0919-0087$01.50/0, 1985.
Atkinson, R.: Atmospheric chemistry of VOCs and NOx, Atmos. Environ., 34, 2063-2101, 10.1016/s1352-2310(99)00460-4, 2000.
Atkinson, R., and Arey, J.: Atmospheric degradation of volatile organic compounds, Chem. Rev., 103, 4605-4638, 10.1021/cr0206420, 2003.
Baker, J., Arey, J., and Atkinson, R.: Formation and reaction of hydroxycarbonyls from the reaction of OH radicals with 1,3-butadiene and isoprene, Environ. Sci. Technol., 39, 4091-4099, 10.1021/es047930t, 2005.
Bonn, B., and Moortgat, G. K.: New particle formation during alpha- and beta-pinene oxidation by O_3, OH and NO_3, and the influence of water vapour: Particle size distribution studies, Atmos. Chem. Phys., 2, 183-196, 10.5194/acp-2-183-2002, 2002.

Bowman, F. M., and Seinfeld, J. H.: Fundamental basis of incremental reactivities of organics in ozone formation in VOC/NOx mixtures. , Atmos. Environ., 28, 3359-3368, 10.1016/1352-2310(94)00165-h, 1994.

Bruns, E. A., Perraud, V., Zelenyuk, A., Ezell, M. J., Johnson, S. N., Yu, Y., Imre, D., Finlayson-Pitts, B. J., and Alexander, M. L.: Comparison of FTIR and particle mass spectrometry for the measurement of particulate organic nitrates, Environ. Sci. Technol., 44, 1056-1061, 10.1021/es9029864, 2010.

Burling, I. R., Yokelson, R. J., Griffith, D. W. T., Johnson, T. J., Veres, P., Roberts, J. M., Warneke, C., Urbanski, S. P., Reardon, J., Weise, D. R., Hao, W. M., and de Gouw, J.: Laboratory measurements of trace gas emissions from biomass burning of fuel types from the southeastern and southwestern United States, Atmos. Chem. Phys., 10, 11115-11130, 10.5194/acp-10-11115-2010, 2010.

Cabanas, B., Baeza, M. T., Salgado, S., Martin, P., Taccone, R., and Martinez, E.: Oxidation of heterocycles in the atmosphere: Kinetic study of their reactions with NO_3 radical, J. Phys. Chem. A, 108, 10818-10823, 10.1021/jp046524t, 2004.

Cao, G., and Jang, M.: An SOA model for toluene oxidation in the presence of inorganic aerosols, Environ. Sci. Technol., 44, 727-733, 10.1021/es901682r, 2010.

Carlton, A. G., Wiedinmyer, C., and Kroll, J. H.: A review of secondary organic aerosol (SOA) formation from isoprene, Atmos. Chem. Phys., 9, 4987-5005, 10.5194/acp-9-4987-2009, 2009.

Chan, A. W. H., Chan, M. N., Surratt, J. D., Chhabra, P. S., Loza, C. L., Crounse, J. D., Yee, L. D., Flagan, R. C., Wennberg, P. O., and Seinfeld, J. H.: Role of aldehyde chemistry and NOx concentrations in secondary organic aerosol formation, Atmos. Chem. Phys., 10, 7169-7188, 10.5194/acp-10-7169-2010, 2010.

Chen, Y., Tong, S., Wang, J., Peng, C., Ge, M., Xie, X., and Sun, J.: The effect of Titanium Dioxide on secondary organic aerosol formation, Environ. Sci. Technol., 52, 11612-11620, 10.1021/acs.est.8b02466, 2018.

Cheng, Y., Zheng, G., Wei, C., Mu, Q., Zheng, B., Wang, Z., Gao, M., Zhang, Q., He, K., Carmichael, G., Poschl, U., and Su, H.: Reactive nitrogen chemistry in aerosol water as a source of sulfate during haze events in China, Sci. Rep., 2, e1601530, 10.1126/sciadv.1601530, 2016.

Cocker, D. R., Mader, B. T., Kalberer, M., Flagan, R. C., and Seinfeld, J. H.: The effect of water on gas-particle partitioning of secondary organic aerosol: II. m-xylene and 1,3,5-trimethylbenzene photooxidation systems, Atmos. Environ., 35, 6073-6085, 10.1016/s1352-2310(01)00405-8, 2001.

Coggon, M. M., Veres, P. R., Yuan, B., Koss, A., Warneke, C., Gilman, J. B., Lerner, B. M., Peischl, J., Aikin, K. C., Stockwell, C. E., Hatch, L. E., Ryerson, T. B., Roberts, J. M., Yokelson, R. J., and de Gouw, J. A.: Emissions of nitrogen-containing organic compounds from the burning of herbaceous and arboraceous biomass: Fuel composition dependence and the variability of commonly used nitrile tracers, Geophys. Res. Lett, 43, 9903-9912, 10.1002/2016gl070562, 2016.

Coury, C., and Dillner, A. M.: A method to quantify organic functional groups and inorganic compounds in ambient aerosols using attenuated total reflectance FTIR spectroscopy and multivariate chemometric techniques, Atmos. Environ., 42, 5923-5932, 10.1016/j.atmosenv.2008.03.026, 2008.

Deng, W., Liu, T., Zhang, Y., Situ, S., Hu, Q., He, Q., Zhang, Z., Lu, S., Bi, X., Wang, X., Boreave, A., George, C., Ding, X., and Wang, X.: Secondary organic aerosol formation from photo-oxidation of toluene with NOx and SO2: Chamber simulation with purified air versus urban ambient air as matrix, Atmos. Environ., 150, 67-76, 10.1016/j.atmosenv.2016.11.047, 2017.

Donahue, N. M., Robinson, A. L., and Pandis, S. N.: Atmospheric organic particulate matter: From smoke to secondary organic aerosol, Atmos. Environ., 43, 94-106, 10.1016/j.atmosenv.2008.09.055, 2009.

Duarte, R., Pio, C. A., and Duarte, A. C.: Spectroscopic study of the water-soluble organic matter isolated from atmospheric aerosols collected under different atmospheric conditions, Anal. Chim. Acta, 530, 7-14, 10.1016/j.aca.2004.08.049, 2005.

Edney, E. O., Driscoll, D. J., Speer, R. E., Weathers, W. S., Kleindienst, T. E., Li, W., and Smith, D. F.: Impact of aerosol liquid water on secondary organic aerosol yields of irradiated toluene/propylene/NOx/$(NH_4)_2SO_4$/air mixtures, Atmos. Environ., 34, 3907-3919, 10.1016/s1352-2310(00)00174-6, 2000.

Engelhart, G. J., Hildebrandt, L., Kostenidou, E., Mihalopoulos, N., Donahue, N. M., and Pandis, S. N.: Water content of aged aerosol, Atmos. Chem. Phys., 11, 911-920, 10.5194/acp-11-911-2011, 2011.

Ervens, B., Turpin, B. J., and Weber, R. J.: Secondary organic aerosol formation in cloud droplets and aqueous particles (aqSOA): A review of laboratory, field and model studies, Atmos. Chem. Phys., 11, 11069-11102, 10.5194/acp-11-11069-2011, 2011.

Faust, J. A., Wong, J. P. S., Lee, A. K. Y., and Abbatt, J. P. D.: Role of aerosol liquid water in secondary organic aerosol formation from volatile organic compounds, Environ. Sci. Technol., 51, 1405-1413, 10.1021/acs.est.6b04700, 2017.

Fry, J. L., Kiendler-Scharr, A., Rollins, A. W., Wooldridge, P. J., Brown, S. S., Fuchs, H., Dube, W., Mensah, A., dal Maso, M., Tillmann, R., Dorn, H. P., Brauers, T., and Cohen, R. C.: Organic nitrate and secondary organic aerosol yield from NO_3 oxidation of beta-pinene evaluated using a gas-phase kinetics/aerosol partitioning model, Atmos. Chem. Phys., 9, 1431-1449, 10.5194/acp-9-1431-2009, 2009.

Gao, S., Surratt, J. D., Knipping, E. M., Edgerton, E. S., Shahgholi, M., and Seinfeld, J. H.: Characterization of polar organic components in fine aerosols in the southeastern United States: Identity, origin, and evolution, J. Geophys. Res., 111, 10.1029/2005jd006601, 2006.

Ge, S., Xu, Y., and Jia, L.: Secondary organic aerosol formation from ethyne in the presence of NaCl in a smog chamber, Environ. Chem., 13, 699-710, 10.1071/en15155, 2016.

Ge, S., Xu, Y., and Jia, L.: Secondary organic aerosol formation from ethylene ozonolysis in the presence of sodium chloride, J. Aerosol Sci., 106, 120-131, 10.1016/j.jaerosci.2017.01.009, 2017a.

Ge, S., Xu, Y., and Jia, L.: Secondary organic aerosol formation from propylene irradiations in a chamber study, Atmos. Environ., 157, 146-155, 10.1016/j.atmosenv.2017.03.019, 2017b.

Gilman, J. B., Lerner, B. M., Kuster, W. C., Goldan, P. D., Warneke, C., Veres, P. R., Roberts, J. M., de Gouw, J. A., Burling, I. R., and Yokelson, R. J.: Biomass burning emissions and potential air quality impacts of volatile organic compounds and other trace gases from fuels common in the US, Atmos. Chem. Phys., 15, 13915-13938, 10.5194/acp-15-13915-2015, 2015.

Gloess, A. N., Vietri, A., Wieland, F., Smrke, S., Schoenbaechler, B., Lopez, J. A. S., Petrozzi, S., Bongers, S., Koziorowski, T., and Yeretzian, C.: Evidence of different flavour formation dynamics by roasting coffee from different origins: On-line analysis with PTR-ToF-MS, Int. J. Mass Spectrom., 365, 324-337, 10.1016/j.ijms.2014.02.010, 2014.

Gomez Alvarez, E., Borras, E., Viidanoja, J., and Hjorth, J.: Unsaturated dicarbonyl products from the OH-initiated photo-oxidation of furan, 2-methylfuran and 3-methylfuran, Atmos. Environ., 43, 1603-1612, 10.1016/j.atmosenv.2008.12.019, 2009.

Greenberg, J. P., Zimmerman, P. R., Heidt, L., and Pollock, W.: Hydrocarbon and carbon-monoxide emissions from biomass burning in Brazil., J. Geophys. Res., 89, 1350-1354, 10.1029/JD089iD01p01350, 1984.

Grgic, I., Nieto-Gligorovski, L. I., Net, S., Temime-Roussel, B., Gligorovski, S., and Wortham, H.: Light induced multiphase chemistry of gas-phase ozone on aqueous pyruvic and oxalic acids, Phys. Chem. Chem. Phys., 12, 698-707, 10.1039/b914377g, 2010.

Hallquist, M., Wenger, J. C., Baltensperger, U., Rudich, Y., Simpson, D., Claeys, M., Dommen, J., Donahue, N. M., George, C., Goldstein, A. H., Hamilton, J. F., Herrmann, H., Hoffmann, T., Iinuma, Y., Jang, M., Jenkin, M. E., Jimenez, J. L., Kiendler-Scharr, A., Maenhaut, W., McFiggans, G., Mentel, T. F., Monod, A., Prevot, A. S. H., Seinfeld, J. H., Surratt, J. D., Szmigielski, R., and Wildt, J.: The formation, properties and impact of secondary organic aerosol: Current and emerging issues, Atmos. Chem. Phys., 9, 5155-5236, 10.5194/acp-9-5155-2009, 2009.

Hatch, L. E., Luo, W., Pankow, J. F., Yokelson, R. J., Stockwell, C. E., and Barsanti, K. C.: Identification and quantification of gaseous organic compounds emitted from biomass burning using two-dimensional gas chromatography-time-of-flight mass spectrometry, Atmos. Chem. Phys., 15, 1865-1899, 10.5194/acp-15-1865-2015, 2015.

Hildebrandt, L., Donahue, N. M., and Pandis, S. N.: High formation of secondary organic aerosol from the photo-oxidation of toluene, Atmos. Chem. Phys., 9, 2973-2986, 10.5194/acp-9-2973-2009, 2009.

Hinks, M. L., Montoya-Aguilera, J., Ellison, L., Lin, P., Laskin, A., Laskin, J., Shiraiwa, M., Dabdub, D., and Nizkorodov, S. A.: Effect of relative humidity on the composition of secondary organic aerosol from the oxidation of toluene, Atmos. Chem. Phys., 18, 1643-1652, 10.5194/acp-18-1643-2018, 2018.

IARC: Dry cleaning, some chlorinated solvents and other industrial chemical., IARC Monographs on the Evaluation of Carcinogenic Risk of Chemicals to Humans, 63. International Agency for Research on Cancer, Lyon, France, 558pp, 1995.

Jang, M. S., Czoschke, N. M., Lee, S., and Kamens, R. M.: Heterogeneous atmospheric aerosol production by acid-catalyzed particle-phase reactions, Science, 298, 814-817, 10.1126/science.1075798, 2002.

Jia, L., and Xu, Y.: Effects of relative humidity on ozone and secondary organic aerosol formation from the photooxidation of benzene and ethylbenzene, Aerosol Sci. Tech., 48, 1-12, 10.1080/02786826.2013.847269, 2014.

Jia, L., and Xu, Y.: Ozone and secondary organic aerosol formation from Ethylene-NO (x)-NaCl irradiations under different relative humidity conditions, J. Atmos. Chem., 73, 81-100, 10.1007/s10874-015-9317-1, 2016.

Jia, L., and Xu, Y.: Different roles of water in secondary organic aerosol formation from toluene and isoprene, Atmos. Chem. Phys., 18, 8137-8154, 10.5194/acp-18-8137-2018, 2018.

Jonsson, A. M., Hallquist, M., and Ljungstrom, E.: Impact of humidity on the ozone initiated oxidation of limonene, delta(3)-carene, and alpha-pinene, Environ. Sci. Technol., 40, 188-194, 10.1021/es051163w, 2006.

Kahan, T. F., Ormond, T. K., Ellison, G. B., and Vaida, V.: Acetic acid formation via the hydration of gas-phase ketene under ambient conditions, Chem. Phys.Lett., 565, 1-4, 10.1016/j.cplett.2013.02.030, 2013.

Kamens, R. M., Zhang, H., Chen, E. H., Zhou, Y., Parikh, H. M., Wilson, R. L., Galloway, K. E., and Rosen, E. P.: Secondary organic aerosol formation from toluene in an atmospheric hydrocarbon mixture: Water and particle seed effects, Atmos. Environ., 45, 2324-2334, 10.1016/j.atmosenv.2010.11.007, 2011.

Kanakidou, M., Seinfeld, J. H., Pandis, S. N., Barnes, I., Dentener, F. J., Facchini, M. C., Van Dingenen, R., Ervens, B., Nenes, A., Nielsen, C. J., Swietlicki, E., Putaud, J. P., Balkanski, Y., Fuzzi, S., Horth, J., Moortgat, G. K., Winterhalter, R., Myhre, C. E. L., Tsigaridis, K., Vignati, E., Stephanou, E. G., and Wilson, J.: Organic aerosol and global climate modelling: A review, Atmos. Chem. Phys., 5, 1053-1123, 10.5194/acp-5-1053-2005, 2005.

Koch, B. P., Witt, M. R., Engbrodt, R., Dittmar, T., and Kattner, G.: Molecular formulae of marine and terrigenous dissolved organic matter detected by electrospray ionization Fourier transform ion cyclotron resonance mass spectrometry, Geochim. Cosmochim. Ac., 69, 3299-3308, 10.1016/j.gca.2005.02.027, 2005.

Kostenidou, E., Pathak, R. K., and Pandis, S. N.: An algorithm for the calculation of secondary organic aerosol density combining AMS and SMPS data, Aerosol Sci. Tech., 41, 1002-1010, 10.1080/02786820701666270, 2007.

Kroll, J. H., Ng, N. L., Murphy, S. M., Flagan, R. C., and Seinfeld, J. H.: Secondary organic aerosol formation from isoprene photooxidation, Environ. Sci. Technol., 40, 1869-1877, 10.1021/es0524301, 2006.

Kroll, J. H., and Seinfeld, J. H.: Chemistry of secondary organic aerosol: Formation and evolution of low-volatility organics in the atmosphere, Atmos. Environ., 42, 3593-3624, 10.1016/j.atmosenv.2008.01.003, 2008.

Labouze, E., Honoré, C., Moulay, L., Couffignal, B., and Beekmann, M.: Photochemical ozone creation potentials, Int. J. Life Cycle Ass., 9, 187-195, 10.1016/j.jclepro.2006.03.002, 2004.

Lee, J. H., and Tang, I. N.: Absolute rate constants for the hydroxyl radical reactions with ehtane, furan, and thiophene at roon temperature, J. Chem. Phys., 77, 4459-4463, 10.1063/1.444367, 1982.

Liljegren, J. A., and Stevens, P. S.: Kinetics of the reaction of OH radicals with 3-methylfuran at low pressure, Int. J. Chem. Kinet., 45, 787-794, 10.1002/kin.20814, 2013.

Lim, Y. B., Tan, Y., Perri, M. J., Seitzinger, S. P., and Turpin, B. J.: Aqueous chemistry and its role in secondary organic aerosol (SOA) formation, Atmos. Chem. Phys., 10, 10521-10539, 10.5194/acp-10-10521-2010, 2010.

Lin, Y.-H., Zhang, Z., Docherty, K. S., Zhang, H., Budisulistiorini, S. H., Rubitschun, C. L., Shaw, S. L., Knipping, E. M., Edgerton, E. S., Kleindienst, T. E., Gold, A., and Surratt, J. D.: Isoprene epoxydiols as precursors to secondary organic aerosol formation: Acid-catalyzed reactive uptake studies with authentic compounds, Environ. Sci. Technol., 46, 250-258, 10.1021/es202554c, 2012.

Liu, S., Jia, L., Xu, Y., Tsona, N. T., Ge, S., and Du, L.: Photooxidation of cyclohexene in the presence of SO_2: SOA yield and chemical composition, Atmos. Chem. Phys., 17, 13329-13343, 10.5194/acp-17-13329-2017, 2017.

Liu, T., Huang, D. D., Li, Z., Liu, Q., Chan, M., and Chan, C. K.: Comparison of secondary organic aerosol formation from toluene on initially wet and dry ammonium sulfate particles at moderate relative humidity, Atmos. Chem. Phys., 18, 5677-5689, 10.5194/acp-18-5677-2018, 2018.

Mahowald, N., Ward, D. S., Kloster, S., Flanner, M. G., Heald, C. L., Heavens, N. G., Hess, P. G., Lamarque, J.-F., and Chuang, P. Y.: Aerosol impacts on climate and biogeochemistry, in, Annu. Rev. Env. Resour., 45-74, 2011.

Malm, W. C., Sisler, J. F., Huffman, D., Eldred, R. A., and Cahill, T. A.: Spatial and seasonal trends in particle concentration and optical extinction in the United States J. Geophys. Res., 99, 1347-1370, 10.1029/93jd02916, 1994.

Ng, N., Kroll, J., Chan, A., Chhabra, P., Flagan, R., and Seinfeld, J.: Secondary organic aerosol formation from m-xylene, toluene, and benzene, Atmos. Chem. Phys., 7, 3909-3922, 2007a.

Ng, N. L., Chhabra, P. S., Chan, A. W. H., Surratt, J. D., Kroll, J. H., Kwan, A. J., McCabe, D. C., Wennberg, P. O., Sorooshian, A., Murphy, S. M., Dalleska, N. F., Flagan, R. C., and Seinfeld, J. H.: Effect of NOx level on secondary organic aerosol (SOA) formation from the photooxidation of terpenes, Atmos. Chem. Phys., 7, 5159-5174, 10.5194/acp-7-5159-2007, 2007b.

Ng, N. L., Kroll, J. H., Chan, A. W. H., Chhabra, P. S., Flagan, R. C., and Seinfeld, J. H.: Secondary organic aerosol formation from m-xylene, toluene, and benzene, Atmos. Chem. Phys., 7, 3909-3922, 10.5194/acp-7-3909-2007, 2007c.

Olsson, M.: Wheat straw and peat for fuel pellets - organic compounds from combustion, Biomass Bioenerg., 30, 555-564, 10.1016/j.biombioe.2006.01.005, 2006.

Pan, S., and Wang, L.: Atmospheric Oxidation Mechanism of m-Xylene Initiated by OH Radical, J. Phys. Chem. A, 118, 10778-10787, 10.1021/jp506815v, 2014.

Penkett, S. A.: Chemistry of the natural atmosphere, Nature, 336, 322-322, 10.1038/336322a0, 1988.

Perzon, M.: Emissions of organic compounds from the combustion of oats - a comparison with softwood pellets, Biomass Bioenerg., 34, 828-837, 10.1016/j.biombioe.2010.01.027, 2010.

Pope, C. A., III, Ezzati, M., and Dockery, D. W.: Fine particulate air pollution and life expectancies in the United States: The role of influential observations, J. Air Waste Manage., 63, 129-132, 10.1080/10962247.2013.760353, 2013.

Riva, M., Barbosa, T. D. S., Lin, Y.-H., Stone, E. A., Gold, A., and Surratt, J. D.: Chemical characterization of organosulfates in secondary organic aerosol derived from the photooxidation of alkanes, Atmos. Chem. Phys., 16, 11001-11018, 10.5194/acp-16-11001-2016, 2016.

Sakamoto, Y., Inomata, S., and Hirokawa, J.: Oligomerization reaction of the criegee intermediate leads to secondary organic aerosol formation in ethylene ozonolysis, J. Phys. Chem. A, 117, 12912-12921, 10.1021/jp408672m, 2013.

Sareen, N., Waxman, E. M., Turpin, B. J., Volkamer, R., and Carlton, A. G.: Potential of aerosol liquid water to facilitate organic aerosol formation: Assessing knowledge gaps about precursors and partitioning, Environ. Sci. Technol., 51, 3327-3335, 10.1021/acs.est.6b04540, 2017.

Sarkar, C., Sinha, V., Kumar, V., Rupakheti, M., Panday, A., Mahata, K. S., Rupakheti, D., Kathayat, B., and Lawrence, M. G.: Overview of VOC emissions and chemistry from PTR-TOF-MS measurements during the SusKat-ABC campaign: high acetaldehyde, isoprene and isocyanic acid in wintertime air of the Kathmandu Valley, Atmos. Chem. Phys., 16, 3979-4003, 10.5194/acp-16-3979-2016, 2016.

Sarrafzadeh, M., Wildt, J., Pullinen, I., Springer, M., Kleist, E., Tillmann, R., Schmitt, S. H., Wu, C., Mentel, T. F., and Zhao, D.: Impact of NOx and OH on secondary organic aerosol formation from β-pinene photooxidation, Atmos. Chem. Phys., 16, 11237-11248, 10.5194/acp-16-11237-2016, 2016.

Shafizadeh, F.: Introduction to pyrolysis of biomass, J. Anal. Appl. Pyrol., 3, 283-305, 10.1016/0165-2370(82)80017-x, 1982.

Smith, M. L., Bertram, A. K., and Martin, S. T.: Deliquescence, efflorescence, and phase miscibility of mixed particles of ammonium sulfate and isoprene-derived secondary organic material, Atmos. Chem. Phys., 12, 9613-9628, 10.5194/acp-12-9613-2012, 2012.

Song, C., Na, K. S., and Cocker, D. R.: Impact of the hydrocarbon to NOx ratio on secondary organic aerosol formation, Environ. Sci. Technol., 39, 3143-3149, 10.1021/es0493244, 2005.

Song, C., Zaveri, R. A., Alexander, M. L., Thornton, J. A., Madronich, S., Ortega, J. V., Zelenyuk, A., Yu, X.-Y., Laskin, A., and Maughan, D. A.: Effect of hydrophobic primary organic aerosols on secondary organic aerosol formation from ozonolysis of alpha-pinene, Geophys. Res. Lett, 34, 10.1029/2007gl030720, 2007.

Song, M., Zhang, C., Wu, H., Mu, Y., Ma, Z., Zhang, Y., Liu, J., and Li, X.: The influence of OH concentration on SOA formation from isoprene photooxidation, Sci. Total Environ,, 650, 951-957, 10.1016/j.scitotenv.2018.09.084, 2019.

Spittler, M., Barnes, I., Bejan, I., Brockmann, K. J., Benter, T., and Wirtz, K.: Reactions of NO_3 radicals with limonene and alpha-pinene: Product and SOA formation, Atmos. Environ., 40, S116-S127, 10.1016/j.atmosenv.2005.09.093, 2006.

Sprengnether, M., Demerjian, K. L., Donahue, N. M., and Anderson, J. G.: Product analysis of the OH oxidation of isoprene and 1,3-butadiene in the presence of NO, J. Geophys. Res., 107, 4268, 10.1029/2001jd000716, 2002.

Stockwell, C. E., Yokelson, R. J., Kreidenweis, S. M., Robinson, A. L., DeMott, P. J., Sullivan, R. C., Reardon, J., Ryan, K. C., Griffith, D. W. T., and Stevens, L.: Trace gas emissions from combustion of peat, crop residue, domestic biofuels, grasses, and other fuels: configuration and Fourier transform infrared (FTIR) component of the fourth Fire Lab at Missoula Experiment (FLAME-4), Atmos. Chem. Phys., 14, 9727-9754, 10.5194/acp-14-9727-2014, 2014.

Stockwell, C. E., Veres, P. R., Williams, J., and Yokelson, R. J.: Characterization of biomass burning emissions from cooking fires, peat, crop residue, and other fuels with high-resolution proton-transfer-reaction time-of-flight mass spectrometry, Atmos. Chem. Phys., 15, 845-865, 10.5194/acp-15-845-2015, 2015.

Stockwell, C. E., Jayarathne, T., Cochrane, M. A., Ryan, K. C., Putra, E. I., Saharjo, B. H., Nurhayati, A. D., Albar, I., Blake, D. R., Simpson, I. J., Stone, E. A., and Yokelson, R. J.: Field measurements of trace gases and aerosols emitted by peat fires in Central Kalimantan, Indonesia, during the 2015 El Nino, Atmos. Chem. Phys., 16, 11711-11732, 10.5194/acp-16-11711-2016, 2016.

Strollo, C. M., and Ziemann, P. J.: Products and mechanism of secondary organic aerosol formation from the reaction of 3-methylfuran with OH radicals in the presence of NOx, Atmos. Environ., 77, 534-543, 10.1016/j.atmosenv.2013.05.033, 2013.

Surratt, J. D., Kroll, J. H., Kleindienst, T. E., Edney, E. O., Claeys, M., Sorooshian, A., Ng, N. L., Offenberg, J. H., Lewandowski, M., Jaoui, M., Flagan, R. C., and Seinfeld, J. H.: Evidence for organosulfates in secondary organic aerosol, Environ. Sci. Technol., 41, 517-527, 10.1021/es062081q, 2007.

Takahama, S., Pathak, R. K., and Pandis, S. N.: Efflorescence transitions of ammonium sulfate particles coated with secondary organic aerosol, Environ. Sci. Technol., 41, 2289-2295, 10.1021/es0619915, 2007.

Tapia, A., Villanueva, F., Salgado, M. S., Cabanas, B., Martinez, E., and Martin, P.: Atmospheric degradation of 3-methylfuran: Kinetic and products study, Atmos. Chem. Phys., 11, 3227-3241, 10.5194/acp-11-3227-2011, 2011.

Tuazon, E. C., Alvarado, A., Aschmann, S. M., Atkinson, R., and Arey, J.: Products of the gas-phase reactions of 1,3-butadiene with OH and NO_3 radicals, Environ. Sci. Technol., 33, 3586-3595, 10.1021/es990193u, 1999.

Varutbangkul, V., Brechtel, F. J., Bahreini, R., Ng, N. L., Keywood, M. D., Kroll, J. H., Flagan, R. C., Seinfeld, J. H., Lee, A., and Goldstein, A. H.: Hygroscopicity of secondary organic aerosols formed by oxidation of cycloalkenes, monoterpenes, sesquiterpenes, and related compounds, Atmos. Chem. Phys., 6, 2367-2388, 10.5194/acp-6-2367-2006, 2006.

Villanueva, F., Barnes, I., Monedero, E., Salgado, S., Gómez, M. V., and Martin, P.: Primary product distribution from the Cl-atom initiated atmospheric degradation of furan: Environmental implications, Atmos. Environ., 41, 8796-8810, 10.1016/j.atmosenv.2007.07.053, 2007.

Villanueva, F., Cabañas, B., Monedero, E., Salgado, S., Bejan, I., and Martin, P.: Atmospheric degradation of alkylfurans with chlorine atoms: Product and mechanistic study, Atmos. Environ., 43, 2804-2813, 10.1016/j.atmosenv.2009.02.030, 2009.

Walser, M. L., Desyaterik, Y., Laskin, J., Laskin, A., and Nizkorodov, S. A.: High-resolution mass spectrometric analysis of secondary organic aerosol produced by ozonation of limonene, Phys. Chem. Chem. Phys., 10, 1009-1022, 10.1039/b712620d, 2008.

Wang, Y., Luo, H., Jia, L., and Ge, S.: Effect of particle water on ozone and secondary organic aerosol formation from benzene-NO_2-NaCl irradiations, Atmos. Environ., 140, 386-394, 10.1016/j.atmosenv.2016.06.022, 2016.

Xu, J., Griffin, R. J., Liu, Y., Nakao, S., and Cocker, D. R., III: Simulated impact of NOx on SOA formation from oxidation of toluene and m-xylene, Atmos. Environ., 101, 217-225, 10.1016/j.atmosenv.2014.11.008, 2015.

Yu, K.-P., Lin, C.-C., Yang, S.-C., and Zhao, P.: Enhancement effect of relative humidity on the formation and regional respiratory deposition of secondary organic aerosol, J. Hazard. Mater., 191, 94-102, 10.1016/j.jhazmat.2011.04.042, 2011.

Zhang, H., Lin, Y.-H., Zhang, Z., Zhang, X., Shaw, S. L., Knipping, E. M., Weber, R. J., Gold, A., Kamens, R. M., and Surratt, J. D.: Secondary organic aerosol formation from methacrolein photooxidation: Roles of NOx level, relative humidity and aerosol acidity, Environ. Chem., 9, 247-262, 10.1071/en12004, 2012.

Zhang, Q., Jimenez, J. L., Canagaratna, M. R., Ulbrich, I. M., Ng, N. L., Worsnop, D. R., and Sun, Y.: Understanding atmospheric organic aerosols via factor analysis of aerosol mass spectrometry: A review, Anal. Bioanal. Chem., 401, 3045-3067, 10.1007/s00216-011-5355-y, 2011.

Zhou, Y., Zhang, H., Parikh, H. M., Chen, E. H., Rattanavaraha, W., Rosen, E. P., Wang, W., and Kamens, R. M.: Secondary organic aerosol formation from xylenes and mixtures of toluene and xylenes in an atmospheric urban hydrocarbon mixture: Water and particle seed effects (II), Atmos. Environ., 45, 3882-3890, 10.1016/j.atmosenv.2010.12.048, 2011.

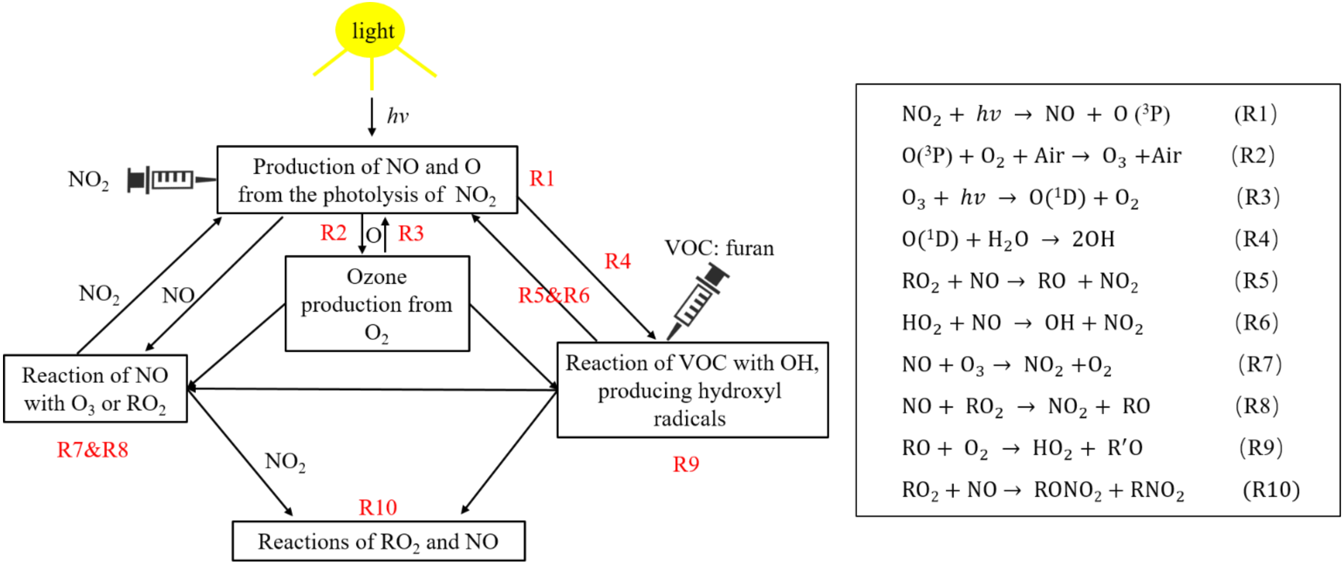

Figure 1: Gas phase inorganic chemical reactions during the experiments.

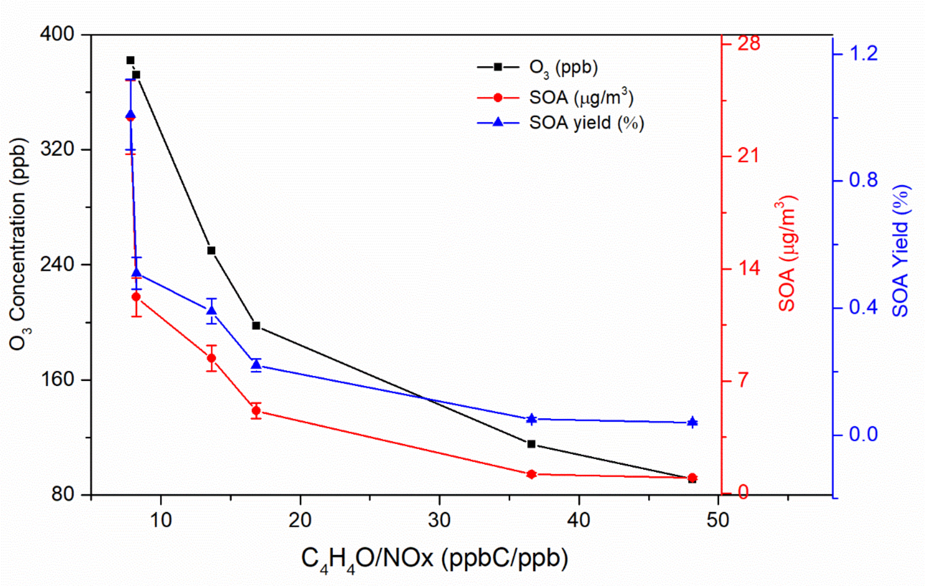

Figure 2: Dependence of the O_3 maximum concentration, SOA mass concentration and SOA yield on the C_4H_4O/NOx ratio. Since the particle wall loss has a weak RH dependence in our chamber, a mean value of 4.7×10^{-5} s^{-1} was used for wall loss correction. A density of 1.4 g cm^{-3} was used in SMPS (Jia and Xu, 2018; Kostenidou et al., 2007).

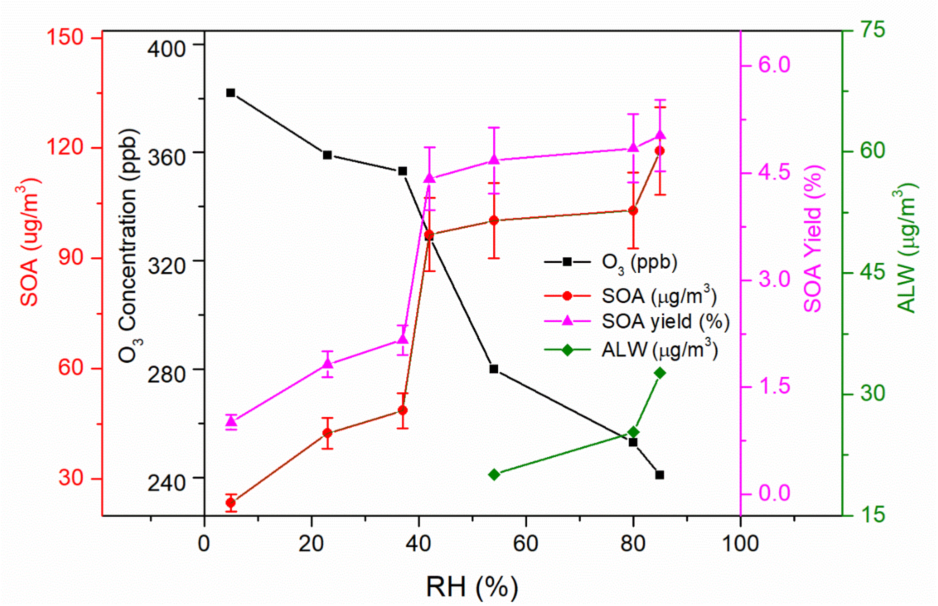

Figure 3: Dependences of O_3 maximum concentration, SOA mass concentration, SOA yield and ALW on relative humidity (RH).

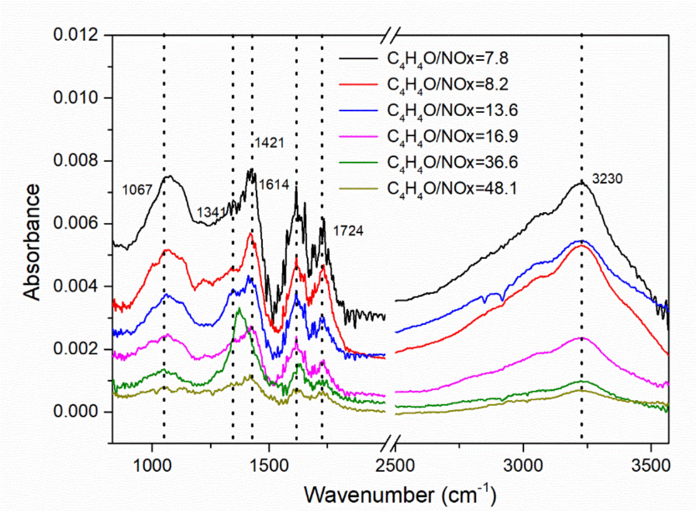

Figure 4: FTIR spectra of particles collected from furan-NOx-NaCl photooxidation experiments with different values of C_4H_4O/NOx ratio ranging from 7.3 to 48.1.

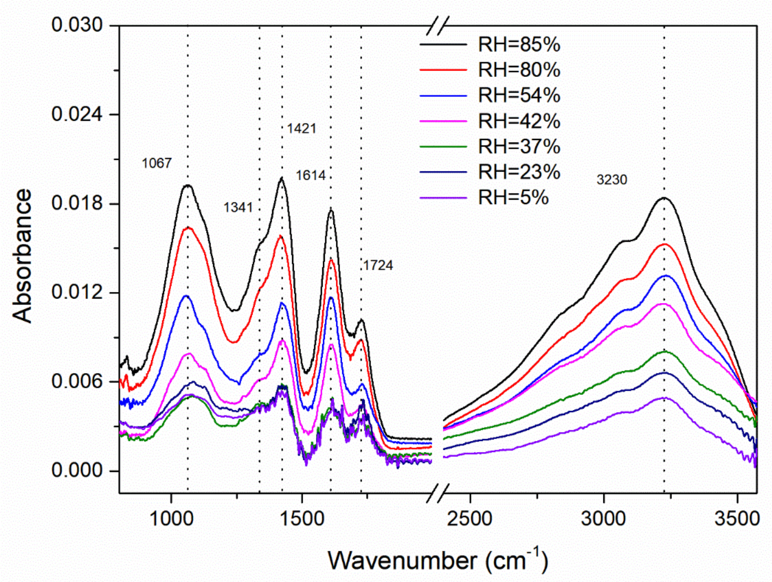

Figure 5: FTIR spectra of particles collected from furan-NOx-NaCl photooxidation experiments with different values of RH ranging from 5 % to 85 %.

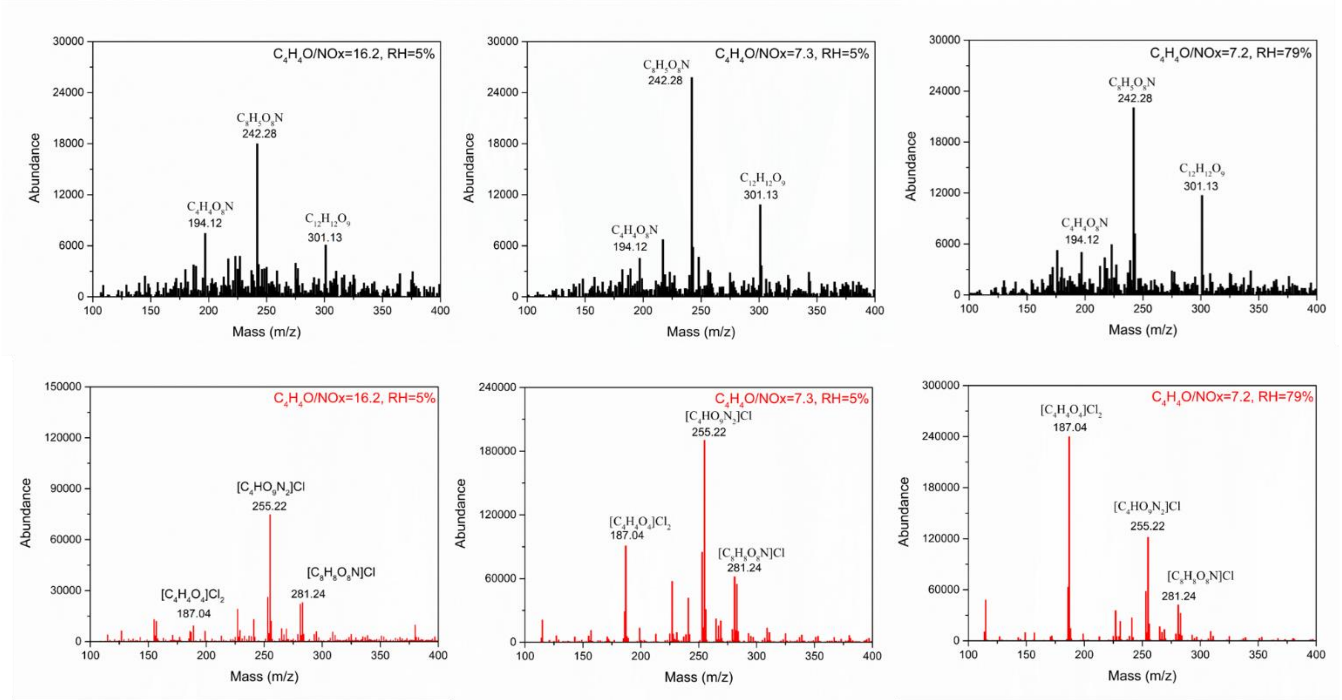

Figure 6: Background-subtracting MS peaks of SOA in both positive ion mode (black) and negative ion mode (red) from the photooxidation of furan under different experimental conditions.

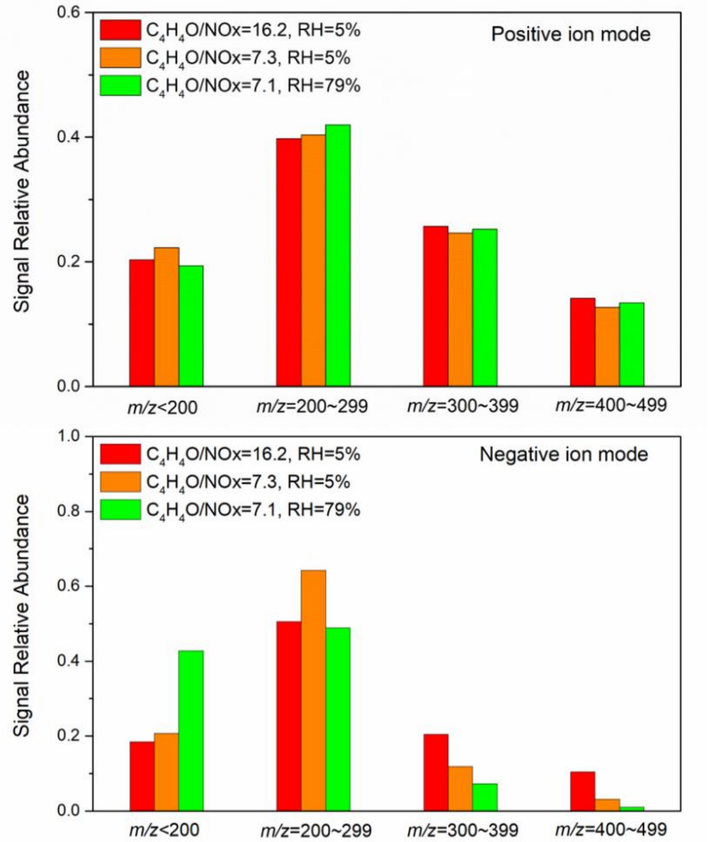

Figure 7: Signal relative abundance of ions detected by ESI-Exactive-Orbitrap MS in both positive and negative ion modes for all ranges of mass-to-charge ratios as identified in this work.

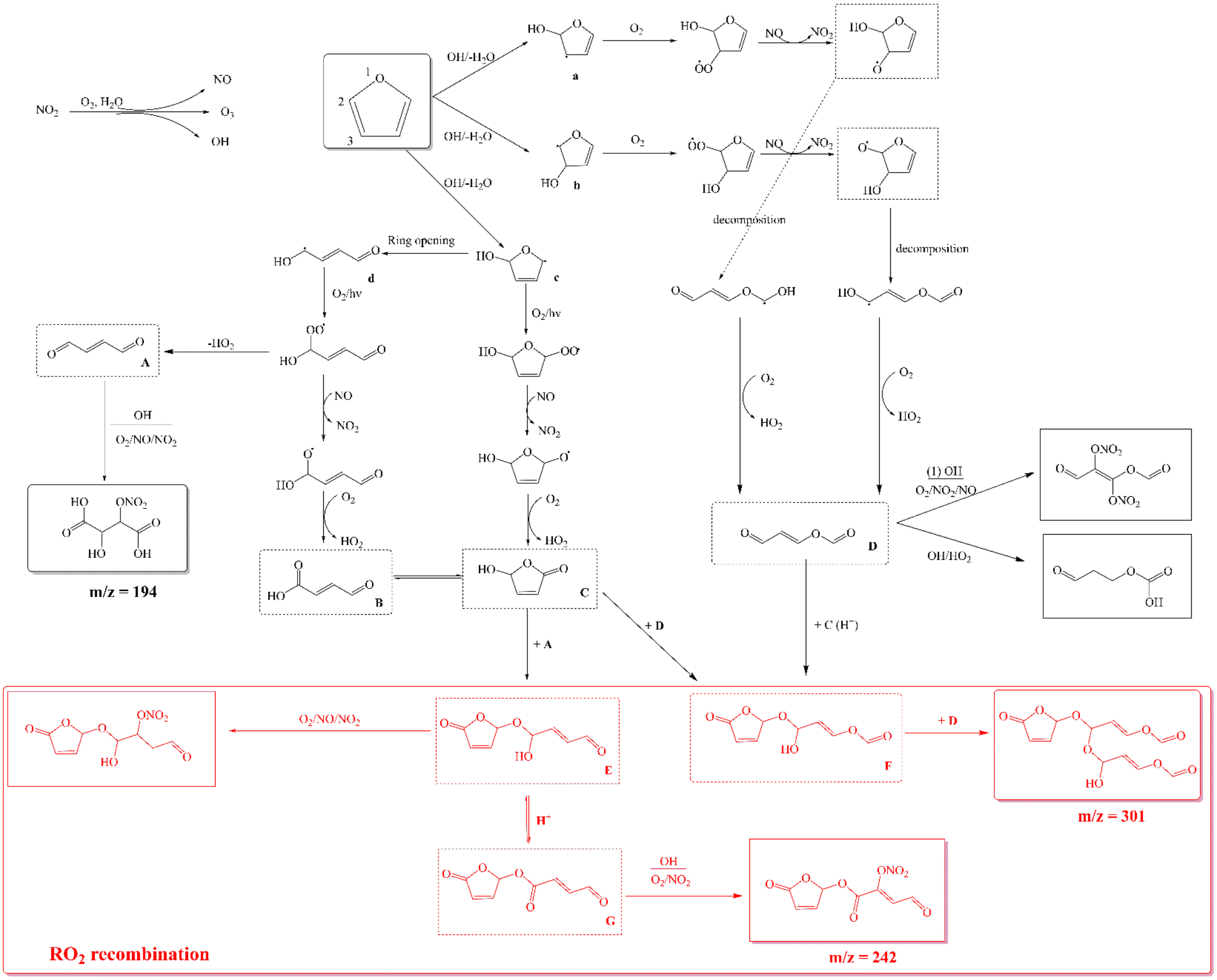

Scheme 1: Proposed mechanism for the SOA formation from furan photooxidation. SOA constituents in dotted and solid boxes are proposed first-generation products and ESI-Exactive-Orbitrap MS detected products, respectively.

Table 1. Summary of initial conditions, O_3 concentrations and particle mass concentrations in furan-NOx-NaCl photooxidation experiments.

Exp No	Initial conditions					SOA formation results						
	$[\text{furan}]_0$ (ppb)	$[NO]_0$ (ppb)	$[NO_2]_0$ (ppb)	RH (%)	C_4H_4O/NOx (ppbC/ppb)	O_3 (ppb)	PM[a] (μg m^{-3})	NaCl[b] (μg m^{-3})	$NaNO_3$[c] (μg m^{-3})	ALW[d] (μg m^{-3})	SOA[e] (μg m^{-3})	SOA yield (%)
1	708.4	2.2	14.6	<5 %	48.1	91	12.2	11.3	3.5	--	1.0±0.1	0.04±0.01
2	749.0	2.0	21.2	<5 %	36.6	115	15.4	10.7	1.6	--	1.2±0.2	0.05±0.01
3	752.5	3.4	41.3	<5 %	16.9	197	21.3	14.1	2.1	--	5.1±0.5	0.3±0.02
4	705.8	5.5	46.3	<5 %	13.6	250	23.5	12.6	2.5	--	8.4±0.9	0.3±0.03
5	783.4	6.9	88.0	<5 %	8.2	372	29.1	13.5	3.9	--	12.2±1.3	0.5±0.05
6	763.4	6.1	91.4	<5 %	7.8	382	38.6	11.5	3.5	--	23.5±2.3	1.0±0.1
7	764.8	4.1	92.6	23 %	7.9	359	55.5	10.4	3.8	--	42.3±4.2	1.9±0.2
8	740.1	2.6	94.7	37 %	7.6	353	64.2	11.2	4.5	--	48.6±4.9	2.2±0.3
9	719.0	5.5	94.7	42 %	7.2	329	111.1	9.4	5.2	--	96.4±9.7	4.5±0.5
10	704.8	3.3	89.6	54 %	7.6	280	138.7	12.0	6.2	20.1	100.2±10.1	4.7±0.4
11	699.3	7.4	95.5	80 %	6.8	253	144.1	8.2	7.6	25.3	103.0±10.3	4.8±0.5
12	780.7	4.7	93.4	85 %	8.0	241	173.0	10.0	11.1	32.6	119.2±10.4	5.0±0.5
13	750.6	3.9	42.6	<5 %	16.2	for ESI-Exactive-Orbitrap MS analysis						
14	723.1	5.8	93.4	<5 %	7.3							
15	740.3	7.4	95.5	79 %	7.1							

[a] PM: particle mass concentration in the chamber was determined from the SMPS and was the sum of NaCl, $NaNO_3$, ALW, and SOA at the end of the experiments.22

[b] NaCl: the amount of NaCl at the end of the experiments;

[c] $NaNO_3$: the amount of $NaNO_3$ at the end of the experiments;

[d] ALW: the amount of aerosol liquid water content at the end of the experiments;

[e] SOA: the amount of secondary organic aerosol at the end of the experiments.

Table 2. Assignment of the observed FTIR absorption frequencies (cm^{-1}).

Absorption frequencies	Functional group	Assignment
1222-868	C-C and C−O	Stretching in alcohols (Coury and Dillner, 2008) C−O of COOH group (Duarte et al., 2005)
1067	C−O−C	C−O stretching (Jang et al., 2002)
1515-1350	−CH	Bending vibration of −C−H group
1614, 1341	RNO_2	Polar nitro groups (Bruns et al., 2010)
1724	C=O	Stretching vibration in carboxylic acid and ketones
3000-2850	C−H	C−H stretching vibration in the saturated carbon ring
3100-3000	C−H	C−H stretching vibration in unsaturated alkene
3200-2400	O−H	Stretching vibration in carboxyl groups
3100-3500	O−H	Stretching vibration in hydroxyl groups